Biophysical Chemistry, 47 (1993) 241–249
Elsevier Science Publishers B.V., Amsterdam

BIOCHE 01775

Theory for two-photon excitation in pattern photobleaching with evanescent illumination

Zhengping Huang * and Nancy L. Thompson

Department of Chemistry, University of North Carolina, Chapel Hill, NC 27599-3290 (USA)

(Received 14 January 1993; accepted in revised form 13 April 1993)

Abstract

Although the translational diffusion coefficients of proteins embedded in, or tightly bound to, natural and artificial cell membranes have been extensively studied, very little is known about the diffusion of proteins weakly bound to membranes. One method for measuring the diffusion coefficients of weakly bound species is to combine evanescent interference patterns with fluorescence pattern photobleaching recovery (TIR-FPPR). However, this technique is intrinsically limited in that the maximum post-bleach fluorescence change, normalized to the pre-bleach fluorescence, is 0.22. This limitation severely restricts the precision of the data and the applicability of the method. In the theoretical work described herein, it is shown that the maximum fractional fluorescence change in TIR-FPPR with two-photon bleaching and observation would be 0.36. Thus, the use of two-photon excitation in TIR-FPPR would significantly improve the signal-to-noise ratio and would provide more precise measurements of the translational diffusion of proteins weakly bound to surfaces.

Keywords: Total internal reflection, Fluorescence photobleaching recovery; Translational diffusion; Surface diffusion; Protein–membrane interactions

1. Introduction

Although the translational diffusion coefficients of proteins embedded in, or tightly bound to, natural and artificial cell membranes have been extensively studied, very little is known about the diffusion of proteins weakly bound to membranes. A recently developed method for measuring the diffusion coefficients of weakly bound species is to combine evanescent interference patterns with fluorescence pattern photobleaching recovery (TIR-FPPR) [1]. In this method, two totally internally reflected laser beams collide to create a periodic evanescent intensity pattern. The evanescent light is used to excite fluorescent molecules that are weakly adsorbed to the interface and in chemical equilibrium with molecules in an adjacent solution. The fluorescence recovery after photobleaching provides a measure of the surface diffusion coefficient of the weakly adsorbed molecules. TIR-FPPR has been experimentally applied to IgE antibodies in the contact region between rat basophil leukemia cells and supported planar membranes [2], to bovine serum albumin adsorbed to glass coated with poly(methylmethacrylate) [3,4], to vesicle fusion at supported planar membranes [5], to insulin adsorbed at erythrocyte membranes [6], and to bovine prothrombin fragment 1 bound in the Ca^{2+}-specific

* To whom correspondence should be addressed.

manner to negatively charged substrate-supported planar membranes (Z. Huang, K.H. Pearce and N.L. Thompson, unpublished results).

The evanescent interference configuration used in TIR-FPPR is advantageous because of the following features: (1) the evanescent interference patterns are very sharp and have a well-defined spatial profile; (2) the illuminated area is large, resulting in high fluorescence and a reduction of photon noise; (3) the spatial periodicity may be accurately controlled by varying the collision angle; and (4) the period of the evanescent interference is small (0.2–5 μm for typical experimental conditions) so that slow translational motions may be accurately measured. However, TIR-FPPR has an intrinsic limitation that severely restricts the precision of the data: the maximum post-bleach fluorescence change, expressed as a fraction of the pre-bleach fluorescence, is 0.22 (see below).

In the theoretical work described herein, we show that the maximum fractional post-bleach fluorescence change in TIR-FPPR with two-photon bleaching and observation would be much larger (0.36). The larger post-bleach fluorescence change occurs because absorption by two-photon excitation would be proportional to the square of the light intensity [7] and would result in a more sharply peaked evanescent interference pattern. We also show that two-photon absorption should increase the degree to which surface diffusion coefficients can be measured in the presence of appreciable, coexistent surface association and dissociation. Two-photon excitation has recently been used to achieve higher resolution in laser-scanning confocal microscopy [8], to measure new spectroscopic properties with solution-phase fluorescence polarization [9], and to measure the translational diffusion of fluorophores in three-dimensional environments such as the cell cytoplasm [10].

2. Results

2.1. General approach

We assume that two laser beams of vacuum wavelength λ_0 and equal intensities are incident

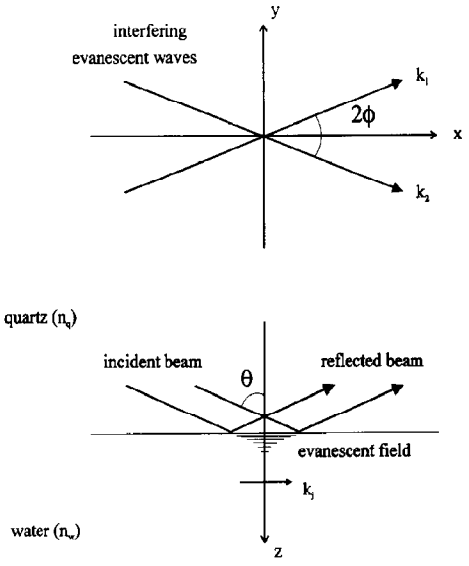

Fig. 1. Optical geometry for TIR-FPPR. Two laser beams are totally internally reflected at a planar interface between quartz and water. The interface is defined as the $x-y$ plane with the x-axis bisecting the two incidence planes. The incidence angle for the two beams is θ, the angle between the two incidence planes is 2ϕ, and $\boldsymbol{k}_1$ and $\boldsymbol{k}_2$ are the propagation vectors of the two evanescent waves.

on a planar interface between quartz and an aqueous solution of fluorescent molecules; that the refractive indices of the quartz and water are $n_q \approx 1.5$ and $n_w \approx 1.3$ over the wavelength range of interest [11,12]; that the beams travel through the quartz towards the interface; that the incidence angles, denoted by θ, are equivalent for the two beams and are greater than the critical angle for total internal reflection; that the beams are either both s-polarized or both p-polarized; that the angle between the two incidence planes, denoted by 2ϕ, is non-zero; that the dielectric interface lies in the x–y plane; and that the x-axis bisects the two lines that correspond to the intersections of the interface and the incidence planes (Fig. 1). For these conditions, the two evanescent fields interfere to produce a spatially periodic evanescent field with an intensity $S(y, z)$ that may be written as [1]

$$S(y, z) = S_a[1 + V\cos(\beta y)]\, e^{-z/d} \qquad (1)$$

In eq. (1), S_a is the average intensity at $z = 0$, V is the visibility (described below), β is the spatial periodicity, d is the evanescent depth, and

$$\beta\lambda_0 = 4\pi n_q \sin\theta \sin\phi \tag{2a}$$

$$\frac{\lambda_0}{d} = 4\pi\sqrt{n_q^2 \sin^2\theta - n_w^2} \tag{2b}$$

Note also in eq. (1), the Gaussian-shaped envelope in the x–y plane is not included in that its characteristic distance is typically much larger than the period of the interference pattern.

For molecules adsorbed to the interface undergoing one-photon absorption, the absorptivity is proportional to $S(y, 0)$. For a two-photon process, the absorptivity is proportional to $S^2(y, 0)$ [7]. The visibility V, or contrast, of the evanescent interference pattern is given by [1]

$$V = \frac{S_{max} - S_{min}}{S_{max} + S_{min}} \tag{3a}$$

$$V_{s,p} = |\cos 2\phi|, \left| \frac{(\sin^2\theta - n^2)\cos 2\phi + \sin^2\theta}{2\sin^2\theta - n^2} \right| \tag{3b}$$

where $n = n_w/n_q$, $S_{max,min}$ refer to the maximum and minimum values of $S(y, 0)$, respectively, and the subscripts p and s refer to the polarization of the incident beams. The square of the evanescent intensity has an apparent visibility V' which is equal to (see eq. 1)

$$V' = \frac{S_{max}^2 - S_{min}^2}{S_{max}^2 + S_{min}^2} = \frac{2V}{1 + V^2} \tag{4}$$

As shown in Fig. 2, $[S(y, 0)/S_{max}]^2$ is more sharply peaked than $[S(y, 0)/S_{max}]$. Mathematically, this result may be seen by noting that $V' \geqslant V$ (eq. 4).

In TIR-FPPR, fluorescent molecules are adsorbed to the quartz/solution interface and are in chemical equilibrium with molecules in the bulk solution. We assume that the surface association constant and site density are large enough so that the evanescently excited fluorescence arises primarily from adsorbed molecules rather than from molecules in solution which are in close proximity to the interface; that the fluorophore absorption dipoles are isotropically oriented and homogeneously distributed in the x–y plane; that the effects of the nearby planar dielectric interface on the angular dependence of the fluorescence emission [13] are negligible; and that the influence of the microscope collection optics on the polarization-sensitive fluorescence collection efficiency [14] is small.

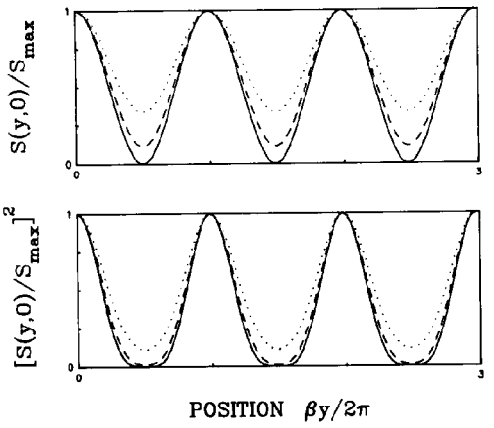

Fig. 2. Normalized evanescent intensities. $S(y, 0)/S_{max}$ and $[S(y, 0)/S_{max}]^2$ were calculated using eq. (1) with $V = 0.5$ (dotted), $V = 0.8$ (dashed) and $V = 1$ (solid). The squared function is sharper and has a higher contrast.

2.2. Surface diffusion without surface kinetics

We first assume that the kinetic dissociation constant is low enough so that fluorescence recovery after photobleaching arises primarily from the exchange of bleached molecules with unbleached molecules through surface diffusion along the interface. The differential equation for the surface concentration of unbleached molecules N, and its initial condition, are

$$\frac{\partial}{\partial t}N(y, t) = D\frac{\partial^2}{\partial y^2}N(y, t) \tag{5a}$$

$$N(y, 0) = \langle N \rangle e^{-A(y)} \tag{5b}$$

where D is the surface diffusion coefficient, $A(y)$ is a bleaching function (described below), and $\langle N \rangle$ is the total surface density of bleached and unbleached fluorophores. Using conventional

Fourier transform methods along with the following expression for the fluorescence normalized to its pre-bleach value

$$F(t) = \frac{\int_0^{2\pi/\beta} O(y)N(y,t)\,dy}{\int_0^{2\pi/\beta} O(y)\langle N\rangle\,dy} \tag{6}$$

where $O(y)$ is an observation function (see below), one finds that

$$F(t) = \left[\frac{1}{\sqrt{4\pi Dt}}\int_0^{2\pi/\beta} dy \int_{-\infty}^{\infty} dy' O(y) \times e^{-A(y')}\, e^{-(y-y')^2/4Dt}\right] \times \left[\int_0^{2\pi/\beta} O(y)\,dy\right]^{-1} \tag{7}$$

where $O(y) = S(y, 0)$ (for one-photon observation) or $O(y) = S^2(y, 0)$ (for two-photon observation), $A(y) = \kappa_1 S(y, 0)$ (for one-photon bleaching) or $A(y) = \kappa_2 S^2(y, 0)$ (for two-photon bleaching), κ_1 and κ_2 are proportionality constants, and the bleach pulse occurs at time $t = 0$.

We denote the fluorescence recovery curve for one-photon photobleaching and one photon observation as $F_{11}(t)$, for two-photon photobleaching and one-photon observation as $F_{21}(t)$, for one-photon photobleaching and two-photon observation as $F_{12}(t)$, and for two-photon photobleaching and two-photon observation as $F_{22}(t)$. These functions may be derived by using eq. (1) (evaluated at $z = 0$) in eq. (7), with the appropriate forms of $A(y)$ and $O(y)$. We find that

$$F_{i1}(t) = X_{i0}(\eta_i, V) - VX_{i1}(\eta_i, V)\, e^{-\beta^2 Dt} \tag{8a}$$

$$F_{i2}(t) = X_{i0}(\eta_i, V) - \frac{4V}{2+V^2}X_{i1}(\eta_i, V)\, e^{-\beta^2 Dt} + \frac{V^2}{2+V^2}X_{i2}(\eta_i, V)\, e^{-4\beta^2 Dt} \tag{8b}$$

where

$$\eta_i \equiv \kappa_i S_a^i \quad \text{for } i = 1, 2 \tag{9a}$$

$$X_{ij}(\eta_i, V) \equiv \frac{(-1)^j}{\pi}\int_0^{\pi} \cos(j\theta)\, e^{-\eta_i(1+V\cos\theta)^i}\,d\theta \quad \text{for } i = 1, 2;\ j = 0, 1, 2 \tag{9b}$$

The expression for $F_{11}(t)$ in eq. (8a) has been published previously [1]. The functions $X_{ij}(\eta_i, V)$ are shown in Fig. 3 for $V = 1$. These functions are generalizations of the modified Bessel functions I_j; i.e., when $i = 1$, $X_{1j} = \exp(-\eta_1)I_j(\eta_1, V)$. The $X_{ij}(\eta_i, V)$ should be common to a variety of problems in two-photon fluorescence microscopy.

In the limit of shallow bleaching ($\eta_1 \ll 1$ or $\eta_2 \ll 1$) and to first order in η_1 or η_2,

$$F_{11}(t) \approx (1-\eta_1) - \tfrac{1}{2}\eta_1 V^2\, e^{-\beta^2 Dt} \tag{10a}$$

$$F_{12}(t) \approx (1-\eta_1) - \frac{2\eta_1 V^2}{2+V^2}\, e^{-\beta^2 Dt} \tag{10b}$$

$$F_{21}(t) \approx 1 - \eta_2\left(1+\tfrac{1}{2}V^2\right) - \eta_2 V^2\, e^{-\beta^2 Dt} \tag{10c}$$

$$F_{22}(t) \approx 1 - \eta_2\left(1+\tfrac{1}{2}V^2\right) - \frac{4\eta_2 V^2}{2+V^2}\, e^{-\beta^2 Dt} - \frac{\eta_2 V^4}{8+4V^2}\, e^{-4\beta^2 Dt} \tag{10d}$$

As shown in eqs. (8), the time dependence of F_{11} and F_{21} (one-photon observation) is expressed as an exponential term with rate $\beta^2 D$. For F_{12} and F_{22} (two-photon observation), there is an additional exponential term with rate $4\beta^2 D$. However, for experimentally reasonable bleaching depths ($0.5 < \eta_i < 1.5$) and times ($t > 0.01/\beta^2 D$), the term with rate $4\beta^2 D$ is negligible (See eqs. 8 and Fig. 3).

It is of interest to characterize the fluorescence recovery curves in terms of experimentally

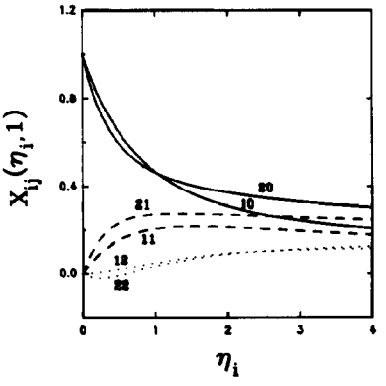

Fig. 3. Functions $X_{ij}(\eta_i, V)$. Shown are the values of $X_{ij}(\eta_i, V)$ for $i = 1$ or $i = 2$ and $j = 0$ (solid), $j = 1$ (dashed) or $j = 2$ (dotted). The curves were calculated using eq. 9b.

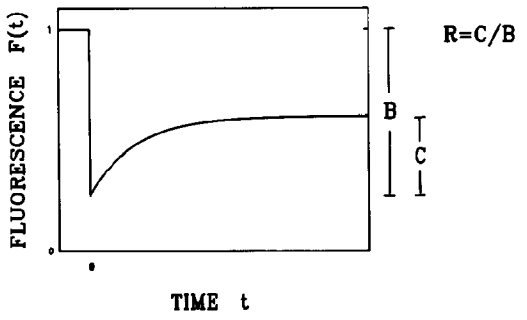

Fig. 4. Relationship of B, C and R to $F(t)$. Shown is a schematic of a TIR-FPPR fluorescence recovery curve. B is the depth of bleach, C is the fractional fluorescence change, and R is the fractional fluorescence recovery. For this theoretical curve, $B = 0.75$, $C = 0.36$ and $R = 0.48$.

accessible parameters. These parameters are the depth of bleach B, the fractional fluorescence change C, and the fractional recovery R and are defined as

$$B = 1 - F(0) \tag{11a}$$

$$C = F(\infty) - F(0) \tag{11b}$$

$$R = C/B \tag{11c}$$

The relationships of B, C and R to $F(t)$ are illustrated in Fig. 4.

Figure 5 shows the predicted values of the fractional fluorescence recovery R as a function of the bleaching parameters η_i and the visibility V for the different types of observation and

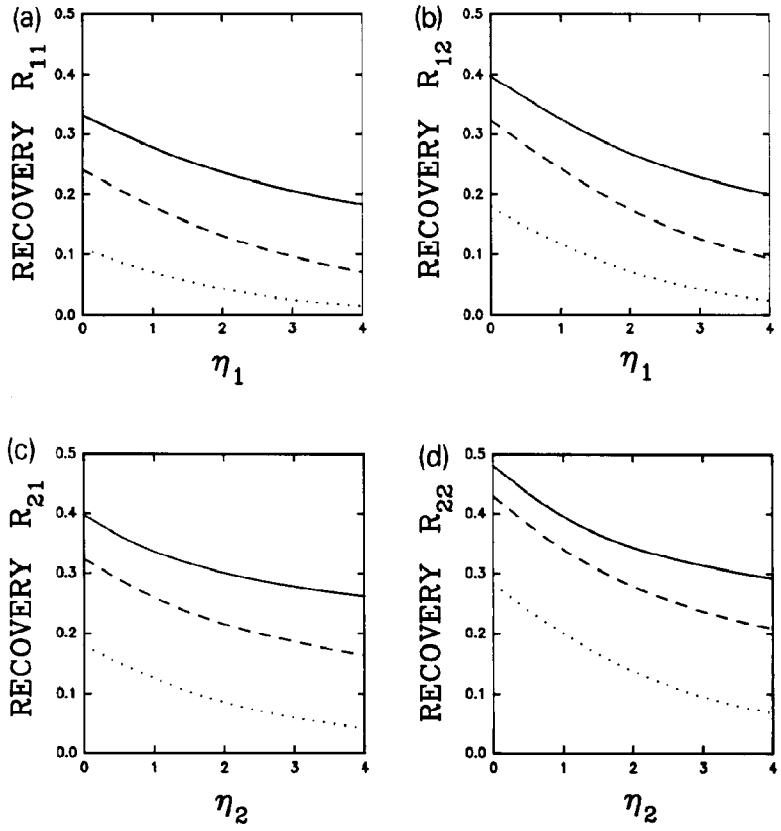

Fig. 5. Dependence of the fractional recovery R on η_i and V. The fractional recovery R increases with the visibility V but decreases with the bleaching parameters η_i. Curves were calculated using eqs. (8), (9) and (11) with $V = 0.5$ (dotted), $V = 0.8$ (dashed) and $V = 1$ (solid).

bleaching. As shown, R is in general lower for deeper bleaching depths (increasing η_1 or η_2) and for imperfect contrast ($V < 1$). However, a key result is that higher values of R are predicted for two-photon observation and bleaching. Using eqs. (8) and (9), one may show that, in the limit of shallow bleaching where the fractional recoveries are maximized,

$$R_{11} = \frac{V^2}{2+V^2} \to \frac{1}{3} \qquad \text{for } V = 1 \tag{12a}$$

$$R_{12} = R_{21} = \frac{2V^2}{2+3V^2} \to \frac{2}{5} \qquad \text{for } V = 1 \tag{12b}$$

$$R_{22} = \frac{16V^2+V^4}{8+24V^2+3V^4} \to \frac{17}{35} \qquad \text{for } V = 1 \tag{12c}$$

The precision of diffusion coefficients measured with TIR-FPPR is related more closely to the fractional fluorescence change, C, than to the fractional recovery, R. For example, although the recovery R is maximized in the limit of very low bleaching, TIR-FPPR data are very noisy in this limit because the net fluorescence change is small. Using eqs. (8) and (11b), one finds that

$$C_{i1} = VX_{i1}(\eta_i, V) \tag{13a}$$

$$C_{i2} = \frac{4V}{2+V^2}X_{i1}(\eta_i, V) - \frac{V^2}{2+V^2}X_{i2}(\eta_i, V) \tag{13b}$$

The values of C calculated from eqs. (13) are shown in Fig. 6 for different values of η_i, V for different types of bleaching and observation. For one-photon bleaching and observation, the maxi-

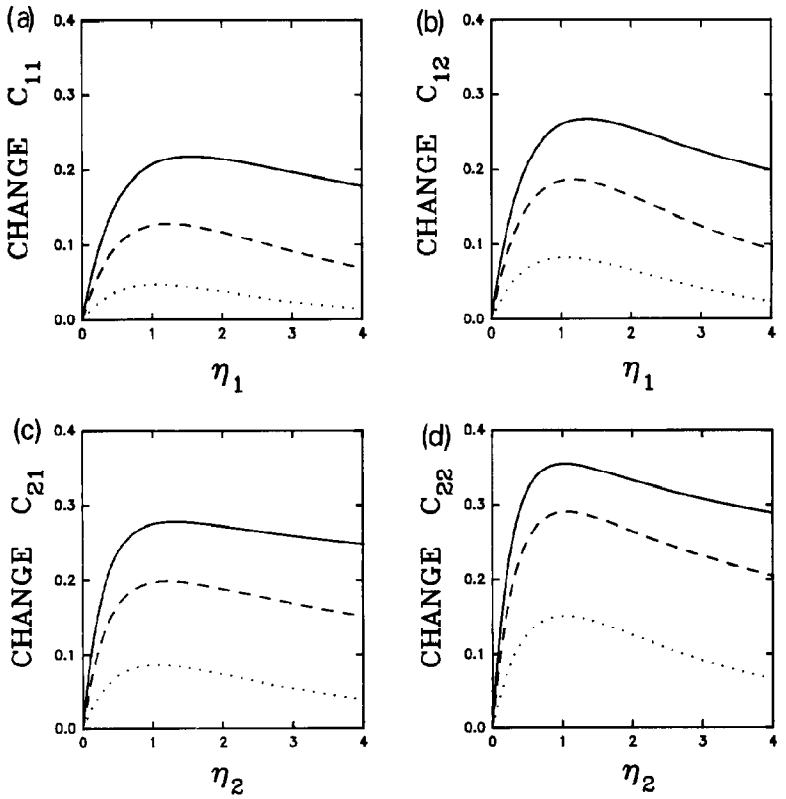

Fig. 6. Dependence of the fractional fluorescence change C on η_i and V. The change C increases with the visibility V and has a maximum with respect to the bleaching parameters η_i. The optimum value of η_1 for one-photon bleaching and observation lies at 1.5, corresponding to $C = 0.22$ while the optimum value of η_2 for two-photon bleaching and observation lies at 1.0, corresponding to $C = 0.36$. The curves were calculated using eqs. (9) and (13) with $V = 0.5$ (dotted), $V = 0.8$ (dashed) and $V = 1$ (solid).

mum value of C is ≈ 0.22 and occurs for $\eta_1 \approx 1.5$. For a mixture of one-photon and two-photon bleaching and observation, the values of C are higher. For two-photon bleaching and observation, the maximum value of C is ≈ 0.36 and occurs for $\eta_2 \approx 1$. Thus, the precision of the data should be improved significantly in a two-photon experiment.

Because the values of R and C shown in Figs. 5 and 6 are plotted as functions of the bleaching parameters η_i rather than the (experimentally measurable) depth of bleach B, it is useful to plot B as a function of η_i and V for different types of observation and bleaching (Fig. 7). For the optimum values of η_1 and η_2, B ranges from 0.8 to 0.9.

2.3. Surface diffusion with surface kinetics

If the fluorescent molecules are bound loosely enough, the fluorescence recovery may in general depend on the kinetic rates for surface association and dissociation, the solution diffusion coefficient, and the surface diffusion coefficient [15]. In the simplest case, the surface reaction occurs between monovalent ligands in solution (P) and

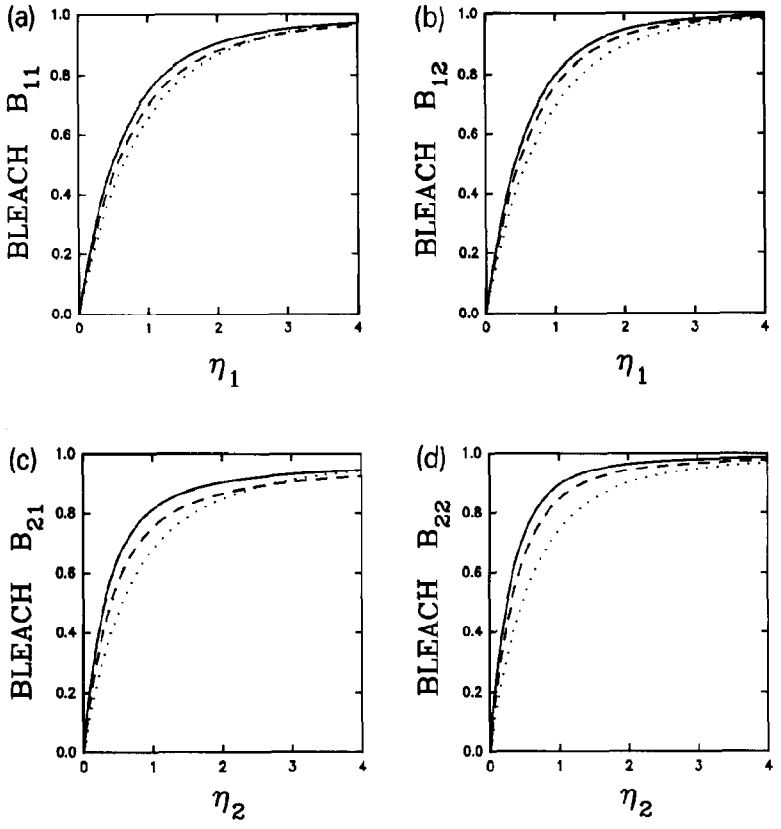

Fig. 7. Dependence of the depth of bleach B on η_i and V. The depths of bleach that correspond to the optimum values of the bleaching parameters ($\eta_1 \approx 1.5$ and $\eta_2 \approx 1.0$) range from 0.8 to 0.9. The curves were calculated using eqs. (8), (9) and (11a) with $V = 0.5$ (dotted), $V = 0.8$ (dashed) and $V = 1$ (solid).

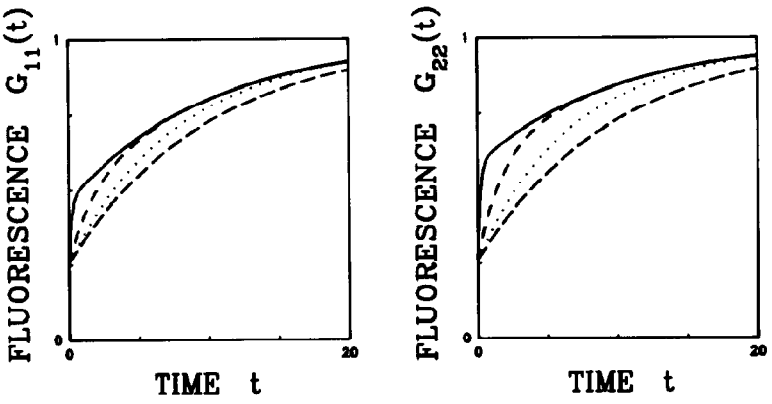

Fig. 8. Fluorescence recovery curves with surface dissociation. Shown on the left is $G_{11}(t)$ (one-photon bleaching and observation) for $\eta_1 = 1$ ($B = 0.74$). Shown on the right is $G_{22}(t)$ (two-photon bleaching and observation) for $\eta_2 = 0.52$ ($B = 0.74$). In both plots, $V = 1$, $k_{off} = 0.1$ and $\beta^2 D = 0$ (long dashed), $\beta^2 D = 0.1$ (dotted), $\beta^2 D = 0.5$ (short dashed) or $\beta^2 D = 5$ (solid). The plots were generated using eqs. (17).

monovalent surface sites (Q) to form surface-bound ligands (N), i .e.,

$$\mathrm{P} + \mathrm{Q} \underset{k_{off}}{\overset{k_{on}}{\rightleftharpoons}} \mathrm{N} \tag{14}$$

where k_{on} and k_{off} are the surface association and dissociation rates, respectively. Furthermore, in the "reaction limit", the fluorescence recovery curve does not depend on the solution diffusion coefficient or the association rate, and the differential equation for $N(y, t)$ is:

$$\frac{\partial N(y,t)}{\partial t} = D\frac{\partial^2}{\partial y^2}N(y,t) + k_{on}\mathrm{PQ} - k_{off}N(y,t) \tag{15}$$

where P and Q are constants.

We define the normalized fluorescence recovery curves for combined surface reaction and diffusion as $G(t)$. Using eqs. (5b), (15) and (6) (with F → G), we than find that

$$G(t) = 1 - \mathrm{e}^{-k_{off}t}(1 - F(t)) \tag{16}$$

where $F(t)$ is given by eq. (7). When k_{off} approaches zero, eq. (16) reduces to eq. (7). When D approaches zero, eq. (16) reduces to a previously published form, i.e., $G(t) = 1 - B \exp(-k_{off}t)$ [15]. Thus, for combined surface reaction and diffusion (eqs. 16 and 8),

$$G_{11}(t) = 1 - \mathrm{e}^{-k_{off}t}\left[1 - X_{10}(\eta_1, V) + VX_{11}(\eta_1, V)\,\mathrm{e}^{-\beta^2 Dt}\right] \tag{17a}$$

$$G_{22}(t) = 1 - \mathrm{e}^{-k_{off}t}\left[1 - X_{20}(\eta_2, V) + \frac{4V}{2+V^2}X_{21}(\eta_2, V)\,\mathrm{e}^{-\beta^2 Dt} - \frac{V^2}{2+V^2}X_{22}(\eta_2, V)\,\mathrm{e}^{-4\beta^2 Dt}\right] \tag{17b}$$

Equation (17a) agrees with a previously published expression [1].

As shown in Fig. 8, the dual modes for fluorescence recovery (replacement of surface-bound, bleached molecules by either surface diffusion or surface dissociation) complicate $G(t)$ and make extraction of D from experimental data difficult. However, the effect of surface diffusion is larger for two-photon bleaching and observation (G_{22}) than for one-photon bleaching and observation (G_{11}). Thus, obtaining lateral diffusion information from TIR-FPPR data when appreciable sur-

face dissociation occurs should be more tractable in a two-photon experiment.

3. Summary

We have shown that by using two-photon absorption in TIR-FPPR, one can expect to obtain data with better precision. When lateral diffusion alone contributes to fluorescence recovery, the fractional fluorescence change will be higher. When recovery occurs from a mixture of surface diffusion and surface binding kinetics, the surface diffusion process will contribute more to the fluorescence recovery. Thus, using two-photon absorption in TIR-FPPR may provide some of the first precise measurements of the translational diffusion coefficients of proteins weakly bound to surfaces.

Acknowledgements

This work was supported by NIH Grant GM-37145 and by NSF Grant DMB-9024028.

References

1 J.R. Abney, B.A. Scalettar and N.L. Thompson, Biophys. J. 61 (1992) 542–552.
2 R.M. Weis, K. Balakrishnan, B.A. Smith and H.M. McConnell, J. Biol. Chem. 257 (1982) 6440–6445.
3 R.D. Tilton, A.P. Gast and C.R. Robertson, Biophys. J. 58 (1990) 1321–1326.
4 R.D. Tilton, C.R. Robertson and A.P. Gast, J. Coll. Int. Sci. 137 (1990) 192–203.
5 E. Kalb, S. Frey and L.K. Tamm, Biochim. Biophys. Acta 1103 (1992) 307–316.
6 D. Axelrod, E.H. Hellen and R.M. Fulbright, Total internal reflection fluorescence, in: Topics in Fluorescence Spectroscopy Volume 3, ed. J.R. Lakowicz, (Plenum Press, New York, 1992) pp. 189–343.
7 R.R. Birge, Acc. Chem. Res. 19 (1986) 138–146.
8 W. Denk, J.H. Strickler and W.W. Webb, Science 248 (1990) 73–76.
9 J.R. Lakowicz and I. Gryczynski, Biophys. Chem. 45 (1992) 1–6.
10 D.W. Piston, E.-S. Wu and W.W. Webb, Biophys. J. 61 (1992) A34.
11 N.J. Harrick, Internal reflection spectroscopy (Harrick Scientific Corporation, Ossining, NY, 1967) p. 140.
12 I. Thormählen, J. Straub and U. Grigull, J. Phys. Chem. Ref. Data 14 (1985) 933–945.
13 E.H. Hellen and D. Axelrod, J. Opt. Soc. Am. B4 (1987) 337–350.
14 D. Axelrod, Meth. Cell Biol. 30 (1989) 333–352.
15 N.L. Thompson, T.P. Burghardt and D. Axelrod, Biophys. J. 33 (1981) 435–454.